

Strong, Ductile Magnesium-Zinc Nanocomposites

MICHAEL DE CICCO, HIROMI KONISHI, GUOPING CAO, HONG SEOK CHOI, LIH-SHENG TURNG, JOHN H. PEREPEZKO, SINDO KOU, RODERIC LAKES, and XIAOCHUN LI

Incorporated SiC nanoparticles are demonstrated to influence the solidification of magnesium-zinc alloys resulting in strong, ductile, and castable materials. By ultrasonically dispersing a small amount (less than 2 vol pct) of SiC nanoparticles, both the strength and ductility exhibit marked enhancement in the final casting. This unusual ductility enhancement is the result of the nanoparticles altering the selection of intermetallic phases. Using transmission electron microscopy (TEM), the MgZn₂ phase was discovered among SiC nanoparticle clusters in hypoeutectic compositions. Differential thermal analysis showed that the MgZn₂ formation resulted in elimination of other intermetallics in the Mg-4Zn nanocomposite and reduced their formation in Mg-6Zn and Mg-8Zn nanocomposites.

DOI: 10.1007/s11661-009-0013-0

© The Minerals, Metals & Materials Society and ASM International 2009

I. INTRODUCTION

RECENT work has shown a significant enhancement in metal matrix composite strength with the addition of nanoelements (*e.g.*, nanoparticles).^[1-4] Applications that have been targeted to date include structural components in the automotive and aerospace industries.^[3] Creating new lightweight, high-strength materials could result in significant weight reductions and energy savings.^[5] Currently restricting wide usage of these materials is the cost of materials synthesis and processing. Most metal matrix nanocomposites (MMNCs) to date are made with expensive powder metallurgy, ball milling, deposition, and infiltration techniques.^[3,4,6-9] A robust solidification processing route has the potential for greatly reducing the cost of MMNC production, making them more attractive materials for a wide range of applications.

However, producing MMNCs can be difficult owing to the high specific surface area and the poor wetting of ceramic nanoparticles by molten metals. Effective dispersion and stabilization of nanoelements in liquids is extremely challenging. Agglomeration and clustering commonly occur,^[10] resulting in poor physical properties. Current solidification processing methods for MMNCs are limited in size and geometric complexity, preventing designers from achieving the design flexibility desired for complex structures (*e.g.*, engine blocks). Recently, Lan *et al.*^[11] and Yang *et al.*^[12,13] developed a

new technique that combined solidification processing (*e.g.*, casting) with an ultrasonic cavitation based dispersion of nanoparticles in metal melts. Nanoparticle reinforced magnesium and aluminum alloys were successfully fabricated. Experimental results show a nearly uniform distribution and good dispersion of the SiC nanoparticles within the metal matrix, resulting in significantly improved mechanical strength while maintaining useful ductility.^[11-13] It was reported^[14] that ultrasonic cavitation can produce transient (in the order of nanoseconds) micro “hot spots” that can have temperatures of about 5000 °C, pressures above 100 MPa, and heating and cooling rates above 10¹⁰ °C/s. The locally extreme conditions induced by the ultrasound can effectively disperse nanoparticles into molten metals due to the strong impact during cavitation and enhanced nanoparticle wettability. Additionally, the nanoparticle dispersion is maintained during solidification even after the ultrasonic vibration is removed.^[12] While MMNCs have shown great strength improvement, to date, little work has been done on the effects nanoparticles have on the solidification of the matrix alloy or tailoring properties in addition to strengthening. This article illustrates the impact of the nanoparticles on matrix solidification and the resulting unusual enhancement of ductility. The material behavior demonstrated in the current work has the potential to allow for highly tailored material structures and material properties by altering intermetallic formation.

II. EXPERIMENTAL PROCEDURE

For this study, three Mg-Zn alloy based MMNCs were prepared and cast. Mg-4Zn (4 wt pct Zn) and Mg-6Zn samples were prepared with 1.5 wt pct β -SiC nanoparticles (Nanostructured and Amorphous Materials Incorporated, Houston, TX, 50-nm average diameter and 99 pct purity). Mg-8Zn alloy samples were prepared with 3 wt pct β -SiC nanoparticles. Reference

MICHAEL DE CICCO, Graduate Research Assistant, HIROMI KONISHI, GUOPING CAO, and HONG SEOK CHOI, Research Associates, and LIH-SHENG TURNG and XIAOCHUN LI, Professors, Department of Mechanical Engineering, JOHN H. PEREPEZKO and SINDO KOU, Professors, Department of Materials Science and Engineering, and RODERIC LAKES, Professor, Department of Engineering Physics, are with the University of Wisconsin-Madison, Madison, WI 53706. Contact e-mail: xclic@engr.wisc.edu

Manuscript submitted November 16, 2008.

Article published online October 14, 2009

samples of Mg-4Zn, Mg-6Zn, and Mg-8Zn were also prepared. The alloys were made by bringing pure magnesium to the liquid state at a temperature of 700 °C. Pure zinc ingot was then added in the appropriate amount for the desired composition. Manual mixing was used to ensure a homogeneous alloy composition. In preparing the MMNC samples, SiC nanoparticles were fed into the melt through a steel tube and dispersed using an ultrasonic power probe. The details of ultrasonic MMNC production have been published elsewhere.^[15] After processing, the melt was cast into bars in a permanent steel mold, which was designed and fabricated according to ASTM B 108-03a. The tensile bars were dog-bone-style tensile bars with a 1.75-in. (44-mm) gage section and a 0.375-in. (9.5-mm) gage section diameter. The bars were tested in a SINTECH 10/GL tensile test frame. For accurate measurement of yield strength at 0.2 pct offset, an extensometer was used for strain measurement up to 1 pct strain at which point the test was paused and the extensometer was removed. Final elongation was measured manually after putting the two test bar pieces back together per ASTM B 557-06.

Cast samples were examined with an optical microscope as well as a LEO 1530 scanning electron microscope (SEM, Carl Zeiss SMT, Inc., Peabody, MA) with energy-dispersive X-ray spectroscopy (EDS) capabilities to determine phase composition. Transmission electron microscopy (TEM) and selected-area electron diffraction (SAED) measurements were obtained with a PHILIPS*

*PHILIP is a trademark of FEI Company, Hillsboro, OR.

CM 200UT microscope (a spherical aberration coefficient (C_s) of 0.5 mm and a point-to-point resolution of 0.19 nm) equipped with an EDS analyzer (Noran Voyager, NORAN Instruments, Inc., Middleton, WI), operated at 200 kV. The TEM samples were polished to 30- μ m thicknesses, mounted on a Mo TEM grid, and ion milled using a RES010 rapid ion beam milling system (E.A. Fischione Instruments, Inc., Export, PA). Milling parameters of a 10 deg angle, 5 kV, and liquid nitrogen to avoid heating effects were used.

X-ray diffraction (XRD) measurements were done using a Scintag Pad V diffractometer (Scintag Inc., Cupertino, CA) with Cu K_α radiation. The alloy samples were embedded in epoxy and final polished with a 1- μ m diamond paste. Scan parameters used were 2θ angle 10 to 80 deg, step size 0.02 deg, and dwell time 12 seconds. Last, a Netzsch STA 409 differential thermal analyzer (DTA, Erich NETZSCH GmbH, Selb, Germany) was used to study melting and solidification behavior at a heating and cooling rate of 10 °C/min.

III. RESULTS AND DISCUSSION

The tensile test results are shown in Table I. For all alloy compositions, the addition of SiC nanoparticles significantly increased yield strength, tensile strength,

Table I. Tensile Results for Mg-Zn Alloys and Nanocomposites; the Asterisks Indicates Data Taken from Only Two Samples, and the Other Data are Taken from Not Less Than Four Samples

Material	0.2 Pct Yield Strength (MPa)	Tensile Strength (MPa)	Elongation at Failure (Pct)
Mg-4Zn	44 ± 2	112 ± 14	5 ± 1
Mg-4Zn + 15 pct SiC	67 ± 4	199 ± 6	10 ± 1
Mg-6Zn	51 ± 4	136 ± 19	5 ± 1
Mg-6Zn + 15 pct SiC	79 ± 5	194 ± 15	7 ± 1
Mg-8Zn*	81	152	3
Mg-8Zn + 3 pct SiC*	111	222	7

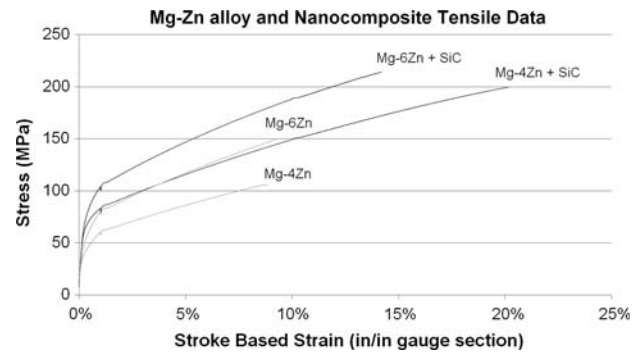
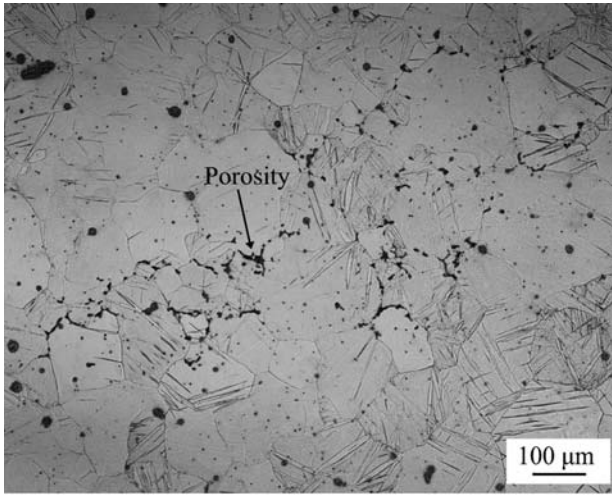


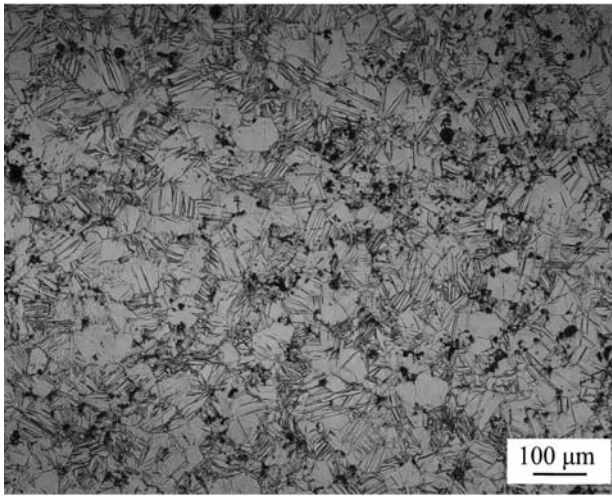
Fig. 1—Tensile test curves for Mg-4Zn and Mg-6Zn alloys and these alloys with 1.5 wt. pct SiC nanoparticle addition showing an increase in maximum stress (strength) and maximum stroke (ductility). Stroke based strain measurement includes strain in the test sample as well as strain due to compliance of the test frame and cannot be taken as the strain in the sample directly. Strain at failure is measured by putting the broken test pieces back together per ASTM B 557-06 to avoid inclusion of test frame compliance in the measurement.

and elongation at failure. The Mg-4Zn + 1.5 pct SiC nanocomposite sample had the greatest increases in strength and ductility relative to the monolithic reference of the compositions tested. Figure 1 shows representative curves from tensile testing. All samples showed the same curve shape indicative of continued strain hardening after yield until failure with little necking. The microstructures of the Mg-4Zn and Mg-4Zn + 1.5 pct SiC samples are shown in Figure 2. The microstructure grain size of the nanocomposite is noticeably refined relative to the monolithic sample. Studies on micron-scale SiC reinforcement of magnesium and magnesium alloys have shown that SiC can act as a nucleation catalyst for primary magnesium grains.^[16] It has also been shown that nanoscale SiC particles can act as nucleation catalysts.^[17] This microstructure refinement is thus likely due to the nucleation catalysis by the SiC nanoparticles.

The mechanisms of nanocomposite strengthening have been studied recently.^[2,19-21] Typically, four strengthening mechanisms are proposed to explain the strength enhancement in MMNCs. They are particle load bearing, enhanced dislocation density in the matrix due to thermal expansion mismatch, Hall-Petch



(a)



(b)

Fig. 2—Optical microscope images of (a) Mg-4Zn and (b) Mg-4Zn + 1.5 pct SiC showing a refined microstructure in the nanocomposite sample, as previously reported by the current authors.^[18]

strengthening due to a refined grain structure, and Orowan strengthening. These can be calculated as

$$\Delta\sigma_{\text{Load}} = 0.5V_p\sigma_m \quad [1]$$

$$\Delta\sigma_D = \sqrt{3}\beta G_m \mathbf{b} \sqrt{\frac{12(T_{\text{process}} - T_{\text{test}})(\alpha_m - \alpha_p)V_p}{\mathbf{b}d_p}} \quad [2]$$

$$\Delta\sigma_{\text{Orowan}} = \frac{0.13G_m \mathbf{b}}{d_p \left[\left(\frac{1}{2V_p} \right)^{1/3} - 1 \right]} \ln \frac{d_p}{2\mathbf{b}} \quad [3]$$

$$\Delta\sigma_{\text{Hall-Petch}} = k_y \left(d_m^{-1/2} - d_c^{-1/2} \right) \quad [4]$$

where the parameters of these expressions are as detailed in Tables II and III. While these individual mechanisms of strengthening are well established and have agreed upon methods for calculation, how these mechanisms interact and form an overall enhancement is not established. Recent works have proposed three different means of calculating the overall enhancement. Goh *et al.*^[21] proposed taking the square root of the sum of the squares of the individual strengthening mechanisms, Zhao *et al.*^[2] proposed adding the individual strengthening enhancements, and Zhang *et al.*^[19,20] proposed a multiplicative method.

The values of $\Delta\sigma_{\text{Load}}$, $\Delta\sigma_D$, $\Delta\sigma_{\text{Orowan}}$, $\Delta\sigma_{\text{Hall-Petch}}$, and $\Delta\sigma_{\text{Experimental}}$ for the Mg-4Zn + 1.5 pct SiC nanocomposite are shown in Table III. As can be seen in the table, the load bearing strengthening in the nanocomposites plays an insignificant role. Combination of the Hall-Petch strengthening and the Orowan strengthening appears to reasonably predict the experimental strengthening. The dislocation density increase due to thermal expansion mismatch, however, predicts a much larger strength enhancement. Regardless of the method used to determine an overall yield strength enhancement, the

Table II. Parameters Used to Determine Predicted Yield Strength Enhancement

Parameter	Description	Value	Reference/Note
α_m	coefficient of thermal expansion of the matrix	$26 \times 10^{-6} \text{ }^\circ\text{C}^{-1}$	—
α_p	coefficient of thermal expansion of the nanoparticles	$4.6 \times 10^{-6} \text{ }^\circ\text{C}^{-1}$	—
β	dislocation strengthening coefficient	1.25	21, 22
σ_m	matrix yield strength	44 MPa	taken from monolithic reference sample experiments
\mathbf{b}	magnitude of the burgers vector	0.32 nm	19
d_c	average grain size in the nanocomposite sample	76 μm	experimentally determined
d_m	average grain size in the monolithic sample	177 μm	experimentally determined
d_p	nanoparticle diameter	50 nm	manufacturer supplied average particle size
G_m	shear modulus of the matrix	15.4 GPa	calculated from experimentally determined tensile modulus
k_y	Hall-Petch material constant	0.133 MPa $\sqrt{\text{m}}$	23
T_{process}	processing temperature	340 $^\circ\text{C}$	solidus temperature
T_{test}	testing temperature	25 $^\circ\text{C}$	room temperature
V_p	volume fraction of nanoparticles	0.0092	calculated from weight fraction

Table III. Predicted Nanocomposite Yield Strength Enhancement Mechanisms and Calculated Values, Compared to the Experimentally Observed Yield Strength Enhancement for the Mg-4Zn + 1.5 Pct SiC Sample

Symbol	Description	Value
$\Delta\sigma_D$	enhancement of nanocomposite yield strength due to dislocation density increase	76 MPa
$\Delta\sigma_{\text{Hall-Petch}}$	enhancement of nanocomposite yield strength due to grain refining	5 MPa
$\Delta\sigma_{\text{Load}}$	enhancement of nanocomposite yield strength due to particle load bearing	0.2 MPa
$\Delta\sigma_{\text{Orowan}}$	enhancement of nanocomposite yield strength due to Orowan strengthening	20 MPa
$\Delta\sigma_{\text{Experimental}}$	experimental yield strength enhancement	23 MPa

large predicted dislocation density increase strengthening exceeds the observed yield strength enhancement. This may be due to a breakdown in assumptions made in developing the model, which was initially developed to describe micron-scale reinforcement.^[22] Assumptions such as the length of dislocations that form being equal to the circumference of the particles may need to be re-examined for application to nanocomposites.

In addition to analysis uncertainty, the models assume conditions that are not necessarily those present in the laboratory. Specifically, annealing was not considered, as the processing temperature for this calculation was 340 °C, the solidus temperature of the alloy. After pouring, the tensile bars cool at a slow rate of approximately 5 °C/min. This allows time at elevated temperatures for annealing to occur reducing the dislocation density. If 0.5 T_{solidus} on an absolute scale is used as the processing temperature in the calculation, the dislocation density increase strengthening reduces to $\Delta\sigma_D = 12$ MPa. Another source of difficulty in applying a predicted yield strength comes from nanoparticle dispersion characteristics. In the model, the nanoparticles are assumed to be perfectly dispersed throughout the melt. However, in the laboratory and in manufacturing processes, perfect dispersion is not achieved.

In the castings, the nanoparticles are well dispersed; however, clusters are still present. Figure 3(a) shows the dispersion of nanoparticles in the Mg-4Zn + 1.5 pct SiC sample. As can be seen in the figure, cluster areas of the nanoparticles are distributed throughout the sample. The EDS mapping of Si (Figure 3(b)) was used to confirm the nanoparticle cluster areas. Image analysis software was then used to determine the area fraction of the nanoparticles. The image analysis showed that the nanoparticle cluster areas accounted for 0.87 pct of the image area. This is close to the total volume fraction of nanoparticles for this sample, 0.91 pct. While the nanoparticles occur primarily in clusters throughout the sample, there is significant penetration of the matrix into the clusters. Figure 4 shows a high-magnification SEM picture of a cluster region. Matrix material can be seen separating the nanoparticles, illustrating that even though the nanoparticles are clustered, they are still wetted by the matrix alloy. This degree of particle dispersion is notably lower than that observed in prior studies when applying the same techniques to nanocomposites based in pure magnesium and aluminum alloys.^[15,26]

While significant strength enhancement in MMNCs is theoretically predicted, ductility is not expected to be

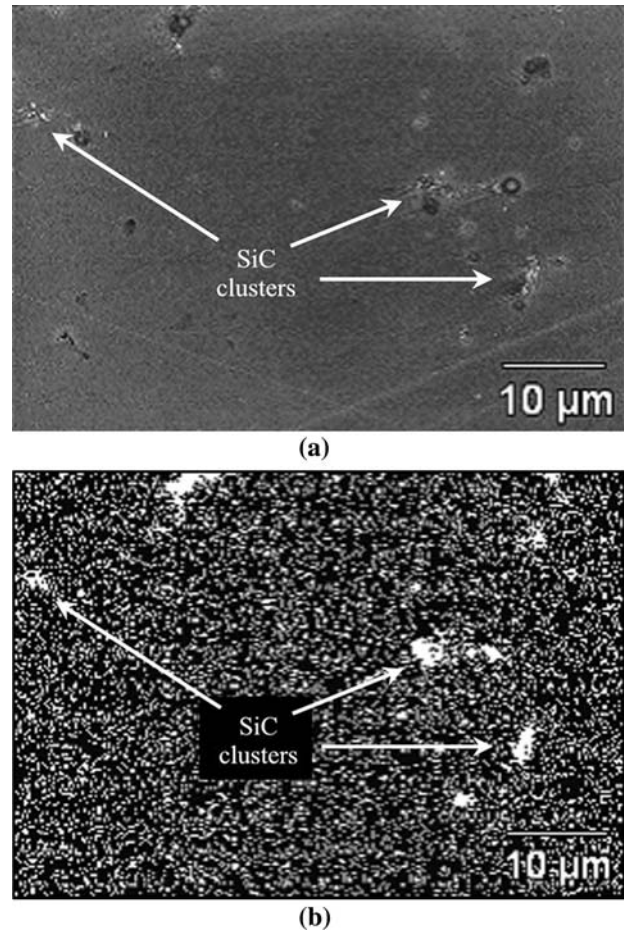


Fig. 3—Particle distribution in a Mg-4Zn + 1.5 pct SiC sample: (a) low-magnification SEM image and (b) EDS mapping of Si, illustrating the areas of nanoparticle concentration in the SEM image.

enhanced. Traditional composites^[27] with microscale reinforcements typically exhibit a reduced ductility. In prior studies with aluminum alloys and AZ91D matrices, nanoparticle composites merely maintain the original ductility.^[11,12,28] Thus, the ductility enhancement seen in Table I and Figure 1 is quite remarkable.

The SEM images of the unreinforced Mg-4Zn and Mg-6Zn samples (Figures 5(a) and (c)) show primarily spherical precipitates dispersed throughout the samples. These precipitates are two-phase regions comprised of the Mg_2Zn_3 and Mg phases. The TEM images, EDS analysis, and diffraction patterns show the two-phase

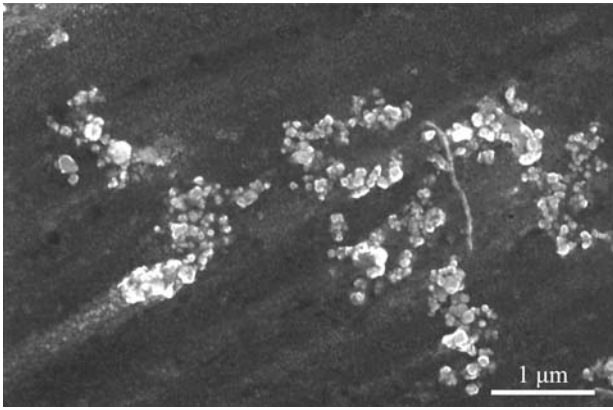


Fig. 4—High-magnification SEM image of a nanoparticle cluster in a Mg-4Zn + 1.5 pct SiC sample.

regions were Mg_2Zn_3 (dark region) and Mg (light region) (Figure 5(e)). This result is consistent with the observations of Gao and Nie.^[29] These two-phase regions were not found in the Mg-4Zn + SiC sample and were only seldom found in the Mg-6Zn + SiC sample (Figures 5(b) and (d)). In the SiC-reinforced samples, the Laves phase, $MgZn_2$, was found among the SiC clusters (Figure 5(f)). The crystal structure of this phase was identified using diffraction patterns, as seen in the inset in the figure. In the unreinforced Mg-8Zn sample, the Mg_7Zn_3 phase was found as well as the two-phase regions of Mg_2Zn_3 and Mg. As can be seen in the phase diagram shown in Figure 6(a), the Mg_7Zn_3 is the equilibrium phase formed by the reaction $L \rightarrow (Mg) + Mg_7Zn_3$. The Mg_7Zn_3 phase then decomposes to form (Mg) and $MgZn$ phases. Gao and Nie report two transition phases in the $Mg_7Zn_3 \rightarrow (Mg) + MgZn$ reaction, one of which has similar structure and composition to the Mg_2Zn_3 phase.^[30] This is one possible route to form the Mg_2Zn_3 phase. Another route is shown in Figure 6(b), where metastable extensions of the (Mg) and Mg_2Zn_3 liquidus lines intersect at a temperature of 336 °C, only 4 deg below the $L \rightarrow (Mg) + Mg_7Zn_3$ eutectic temperature. Below 336 °C, it is possible to have formed Mg_2Zn_3 through a metastable $L \rightarrow (Mg) + Mg_2Zn_3$ reaction.

Thermal results *via* DTA (Figures 7(a) through (f)) support the intermetallic phase formation observed by microscopy. In the Mg-4Zn and Mg-6Zn samples, peaks at 329 °C on cooling are seen. This is consistent with the temperatures where intermetallics are expected to form both the equilibrium Mg_7Zn_3 phase and Mg_2Zn_3 . In the Mg-6Zn sample, a shoulder on the primary peak is seen starting at 340 °C (Figure 7(f)), a possible indicator of Mg_7Zn_3 formation. However, unlike the unreinforced samples, the Mg-4Zn + SiC sample showed solidification had completed before 340 °C, the eutectic temperature (Figure 7(e)). The Mg-6Zn + SiC sample showed a reduction in the 329 °C peak associated with Mg_7Zn_3 or Mg_2Zn_3 formation (Figure 7(f)). However, unlike the Mg-4Zn + SiC sample, the peak was not completely eliminated, indicating small amounts of intermetallics still formed at these temperatures. This is consistent with

the microscopy observations of a small amount of the two-phase region as well as the $MgZn_2$ phase.

In addition to the DTA data showing a suppression of the Mg_7Zn_3 and Mg_2Zn_3 phases, there is evidence for the formation of a new phase. It is evident in Figure 8 that the Mg-4Zn + 1.5 pct SiC sample has a small peak at a temperature of ~565 °C on cooling that is not present in the Mg-4Zn sample. With additional Zn and SiC, the Mg-8Zn + 3 pct SiC sample has a more pronounced peak near the same temperature. To investigate the phase that forms, samples of Mg-8Zn and Mg-8Zn + 3 pct SiC were prepared by cooling slowly from the molten state to 550 °C and then quenching in water to ensure phase preservation. These samples were then examined with XRD to determine the identity of the phase that forms at 565 °C. The XRD results are shown in Figure 9. The monolithic Mg-8Zn sample shows peaks for the Mg_7Zn_3 phase, whereas the Mg-8Zn + 3 pct SiC sample does not. Instead, a peak closely matching the $MgZn_2$ phase appears. While it is difficult to identify a phase from a single peak, it is clear from XRD examination that the nanocomposite sample produces different phases when exposed to the same thermal history as the monolithic sample. Lack of clear evidence of the $MgZn_2$ phase in the XRD results may be due to the small sizes of this phase. Figure 5(f) shows that this phase forms in crystals on the scale of 100 nm. This would cause peak broadening in the XRD results, and a broad peak of a small quantity of $MgZn_2$ could easily be lost in the noise of the signal. Thus, it is possible for the $MgZn_2$ phase to be present. Following the thermodynamic modeling of Miettinen,^[32] the melting temperature of the $MgZn_2$ phase was determined to be 465 °C. Thus, it is unlikely for this phase to account for the peak seen at 565 °C in the DTA curves, further suggesting that $MgZn_2$ is the real source of the peak in the DTA results.

The microscopy and DTA results show that small additions of SiC nanoparticles favor a nanoscale $MgZn_2$ phase suppressing micron-scale Mg_7Zn_3 and Mg_2Zn_3 formation. Moreover, the $MgZn_2$ formation occurs at temperatures well above the melting points of Mg_7Zn_3 and Mg_2Zn_3 , thus consuming the available Zn, eliminating or reducing the Mg_7Zn_3 and Mg_2Zn_3 phases. This reduction in size and quantity of intermetallic phases can reduce stress concentrations in the sample. Converting the intermetallic phases to the nanoscale may change the way in which they interact with the matrix such that the traditional continuum stress concentrating phenomena typical of microscale inclusions no longer operate. This is illustrated by comparison of the ductility enhancement in the Mg-4Zn + SiC and Mg-6Zn + SiC nanocomposites. In the case of the Mg-4Zn + SiC nanocomposite, where microscale intermetallic formation is completely suppressed, as determined from the DTA results, the ductility enhancement is 120 pct compared to the unreinforced alloy. In the Mg-6Zn + SiC nanocomposite, where Mg_7Zn_3 and Mg_2Zn_3 phase suppression is incomplete, the ductility enhancement is smaller, 40 pct. The ability to manipulate intermetallic phase formation *via* nanoparticle addition can lead to optimization of MMNC properties

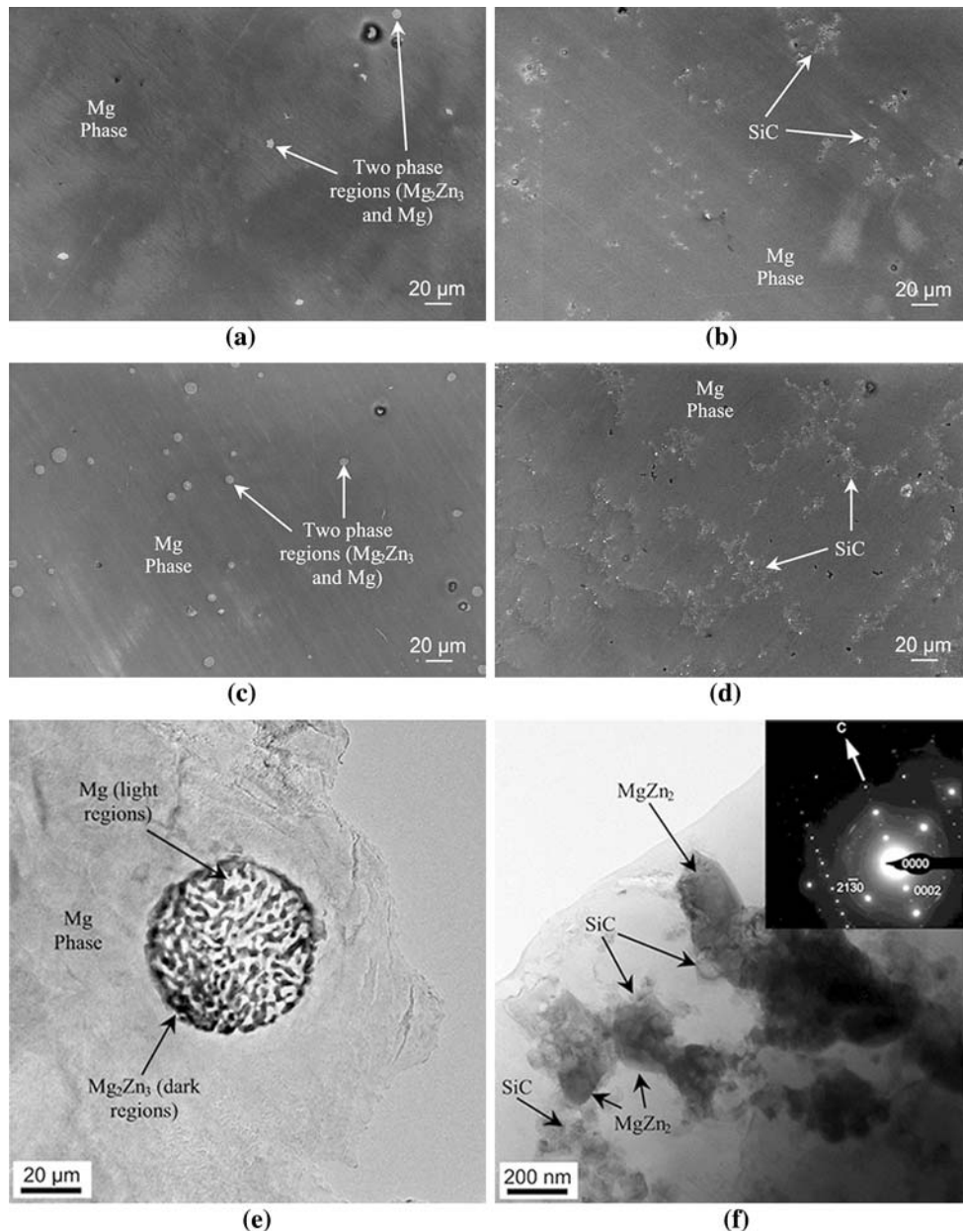


Fig. 5—SEM images showing the features of the (a) Mg-4Zn, (b) Mg-4Zn + 1.5 wt pct SiC nanocomposite, (c) Mg-6Zn, and (d) Mg-6Zn + 1.5 wt pct SiC nanocomposite. The TEM images showing (e) two-phase precipitate in Mg-6Zn and (f) MgZn₂ phase in Mg-6Zn + 1.5 wt pct SiC with SAED pattern of the MgZn₂ area shown in the inset.

other than strength and ductility. Properties such as creep resistance, wear resistance, and high-temperature stability that are impacted significantly by intermetallic phase formation may be greatly modified.

The development of MgZn₂ phase formation in the hypoeutectic Mg-Zn alloys studied is remarkable. Clearly, for bulk compositions in the hypoeutectic range, formation of MgZn₂ at about 565 °C is not possible. At the same time, the MgZn₂ phase is only observed in contact with the SiC nanoparticles. From this observation, it can be speculated that MgZn₂ formation may be promoted by a Zn segregation at the liquid-SiC nanoparticle interface. Another possibility

is for trace impurities such as free Si in the SiC nanoparticles to have altered the intermetallic phase stabilities in the alloy. However, this is unlikely due to the small amounts of nanoparticle addition and the high purity of the nanoparticles (99 pct). It is clear that additional study is needed to resolve the details of the MgZn₂ phase formation. What is quite evident is that the SiC nanoparticle-induced phase selection has a significant impact on the bulk material mechanical properties. The conversion of microscale Mg₇Zn₃ and Mg₂Zn₃ to a nanoscale MgZn₂ alters the size scale and identity of the intermetallic inclusions resulting in a significant increase in ductility.

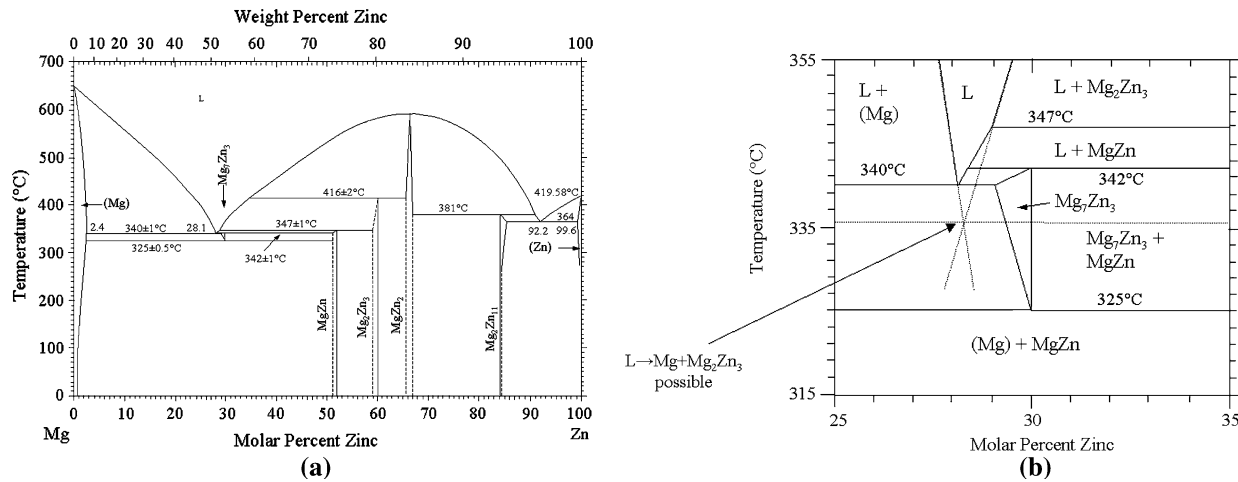


Fig. 6—(a) Mg-Zn phase diagram in its entirety and (b) closer examination of the middle portion of the Mg-Zn phase diagram showing the temperature at which the $L \rightarrow \text{Mg} + \text{Mg}_2\text{Zn}_3$ reaction becomes possible.^[31]

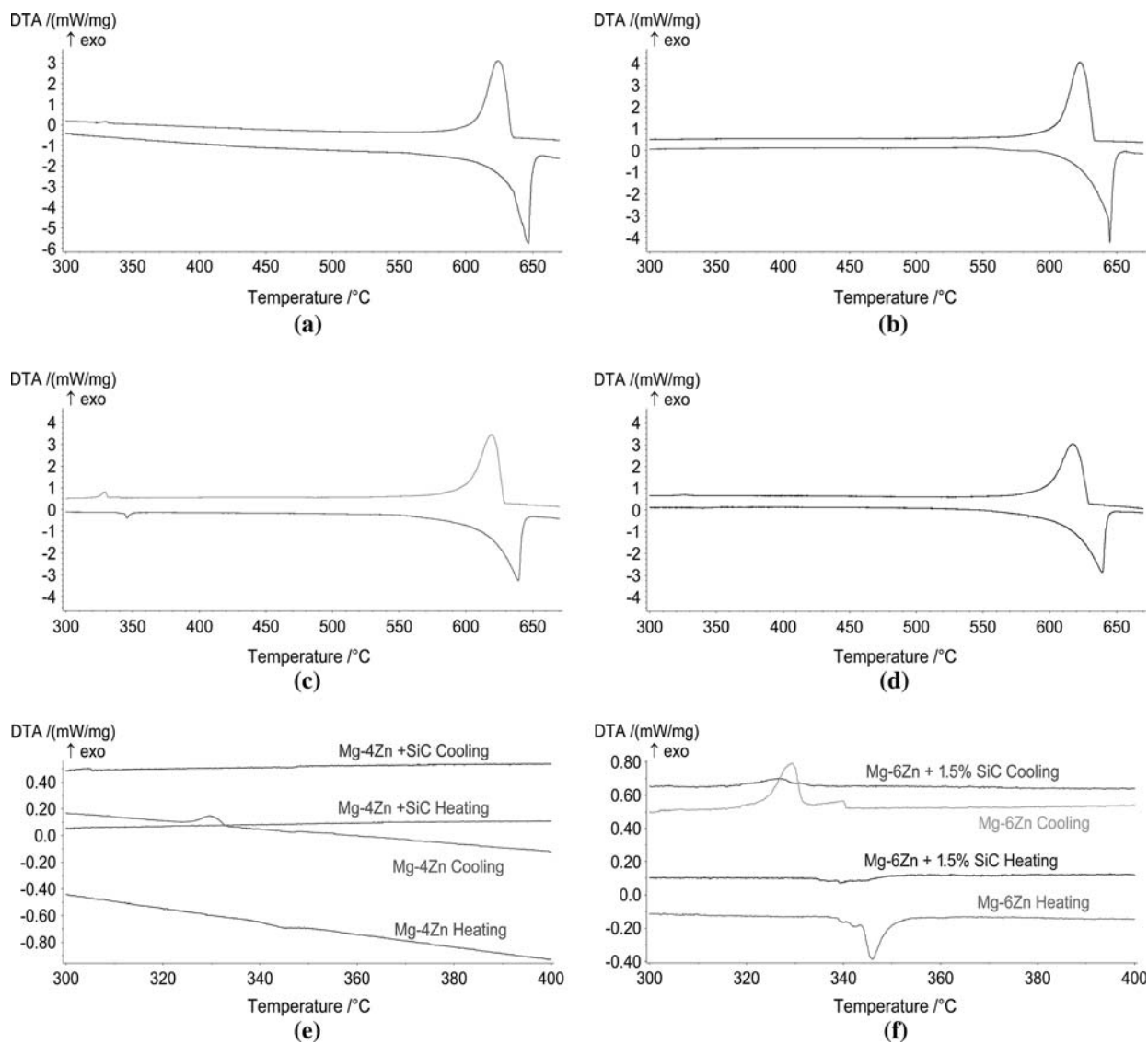


Fig. 7—DTA results for thermal properties: (a) Mg-4Zn, (b) Mg-4Zn + SiC, (c) Mg-6Zn, and (d) Mg-6Zn + SiC. Close examination of the onset of melting and the final solidification in (e) Mg-4Zn and Mg-4Zn + SiC and (f) Mg-6Zn and Mg-6Zn + SiC.

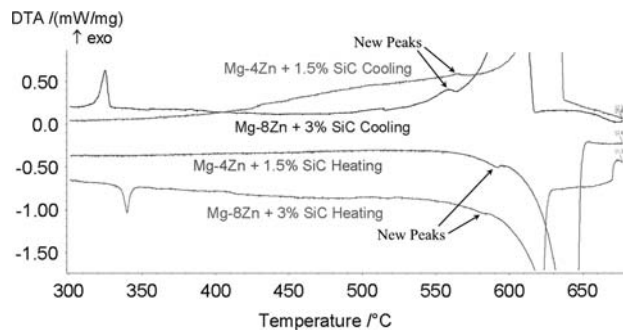


Fig. 8—DTA curves of Mg-4Zn + 1.5 pct SiC and Mg-8Zn + 3 pct SiC samples showing a new peak in the nanocomposites at 560 °C to 590 °C.

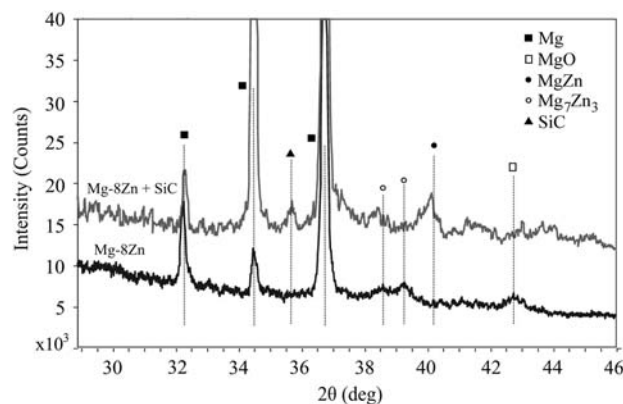


Fig. 9—XRD results from Mg-8Zn and Mg-8Zn + 3 pct SiC samples quenched from 550 °C.

IV. CONCLUSIONS

Mg-Zn based MMNCs with SiC nanoparticle addition were successfully made using ultrasonic processing. These MMNCs showed marked improvement in strength and ductility when compared to unreinforced alloys. The predicted yield strength enhancements from Hall-Petch strengthening and Orowan strengthening were in reasonable agreement with the observed enhancement. The predicted yield strength enhancement from the increase in dislocation density due to thermal expansion mismatch was significantly higher than the observed enhancement. This may be due to annealing during cooling and the nanoparticles not being ideally dispersed, as is assumed in the predicted yield strength. Additionally, the dislocation density model may be failing to capture accurately the nanoscale phenomena occurring, as it was developed for micron-scale reinforcements. The significant and unexpected increase in ductility of the MMNCs was attributed to the nanoparticles suppressing formation of microscale Mg_7Zn_3 and Mg_2Zn_3 in favor of a nanoscale $MgZn_2$ phase. The suppression of the Mg_7Zn_3 and Mg_2Zn_3 phases was verified by SEM observation and thermal analysis. This nanoparticle induced phase manipulation eliminates stress concentrations associated with the comparatively large microscale Mg_7Zn_3 and Mg_2Zn_3 as well as

changing intermetallic phase identity. Nanoparticle induced phase manipulation is a promising way of improving many material properties allowing for highly tailored nanocomposite materials.

REFERENCES

- X.C. Tong and H.S. Fang: *Metall. Mater. Trans. A*, 1998, vol. 29A, pp. 893–902.
- Y.T. Zhao, S.L. Zhang, G. Chen, X.N. Cheng, and C.Q. Wang: *Compos. Sci. Technol.*, 2008, vol. 68, pp. 1463–70.
- S.F. Hassan and M. Gupta: *Mater. Sci. Technol.*, 2004, vol. 20, pp. 1383–88.
- S.F. Hassan and M. Gupta: *J. Compos. Mater.*, 2007, vol. 41, pp. 2533–43.
- R.M. Heavenrich: EPA420-R-06-011, Office of Transportation and Air Quality, U.S. Environmental Protection Agency, Washington, DC, 2006, pp. 1–80.
- A.F. Zimmerman, G. Palumbo, K.T. Aust, and U. Erb: *Mater. Sci. Eng., A*, 2002, vol. 328, pp. 137–46.
- M.J. Tan and X. Zhang: *Mater. Sci. Eng., A*, 1998, vol. 244, pp. 80–85.
- H. Ferkel and B.L. Mordike: *Mater. Sci. Eng., A*, 2001, vol. 298, pp. 193–99.
- D.Y. Ying and D.L. Zhang: *Mater. Sci. Eng., A*, 2000, vol. 286, pp. 152–56.
- Y.S. Kwon, D.V. Dudina, M.A. Korchagin, and O.I. Lomovsky: *J. Mater. Sci.*, 2004, vol. 39, pp. 5325–31.
- J. Lan, Y. Yang, and X. Li: *Mater. Sci. Eng., A*, 2004, vol. 386, pp. 284–90.
- Y. Yang, J. Lan, and X. Li: *Mater. Sci. Eng., A*, 2004, vol. 380, pp. 378–83.
- Y. Yang and X. Li: *J. Manuf. Sci. Eng. Trans. ASME*, 2007, vol. 129, pp. 252–55.
- K.S. Suslick and G.J. Price: *Annu. Rev. Mater. Sci.*, 1999, vol. 29, pp. 295–326.
- G. Cao, H. Konishi, and X. Li: *J. Manuf. Sci. Eng. Trans. ASME*, 2008, vol. 130, pp. 031105.1–031105.6.
- A. Luo: *Can. Metall. Q.*, 1996, vol. 35, pp. 375–83.
- M. De Cicco, L.S. Turng, X. Li, and J.H. Perepezko: *Solid State Phenomena.*, 2008, vols. 141–143, pp. 487–92.
- G. Cao, J. Kobliiska, H. Konishi, and X. Li: *Metall. Mater. Trans. A*, 2008, vol. 39A, pp. 880–86.
- Z. Zhang and D.L. Chen: *Mater. Sci. Eng., A*, 2008, vols. 483–484, pp. 148–52.
- Z. Zhang and D.L. Chen: *Scripta Mater.*, 2006, vol. 54, pp. 1321–26.
- C.S. Goh, J. Wei, L.C. Lee, and M. Gupta: *Acta Mater.*, 2007, vol. 55, pp. 5115–21.
- L.H. Dai, Z. Ling, and Y.L. Bai: *Compos. Sci. Technol.*, 2001, vol. 61, pp. 1057–63.
- ASM Handbook*, vol. 2, *Properties and Selection: Nonferrous Alloys and Special-Purpose Materials, Properties of Magnesium Alloys, Cast Magnesium Alloys*, ASM INTERNATIONAL, Materials Park, OH, 1992, <http://products.asminternational.org/hbk/index.jsp>.
- CoorsTek Inc. website, <http://www.coorstek.com/materials/ceramics/carbides/puresichr.asp>, 2009.
- J. Lin, Q. Wang, L. Peng, Y. Zhou, and W. Ding: *Mater. Sci. Forum*, 2007, vols. 546–549, pp. 319–22.
- M. De Cicco, L. Turng, X. Li, and J.H. Perepezko: *Solid State Phenomena*, 2006, vols. 116–117, pp. 478–83.
- ASM Handbook*, vol. 21, *Composites, Introduction to Composites*, ASM INTERNATIONAL, Materials Park, OH, 1992, <http://products.asminternational.org/hbk/index.jsp>.
- Y. Yang and X. Li: *J. Manuf. Sci. Eng. Trans. ASME*, 2007, vol. 129, pp. 497–501.
- X. Gao and J.F. Nie: *Scripta Mater.*, 2007, vol. 57, pp. 655–58.
- X. Gao and J.F. Nie: *Scripta Mater.*, 2007, vol. 56, pp. 645–48.
- J.B. Clark, L. Zabdyr, and Z. Moser: in *Phase Diagrams of Binary Magnesium Alloys*, A.A. Nayeb-Hashemi and J.B. Clark, eds., ASM INTERNATIONAL, Metals Park, OH, 1988, pp. 353–64.
- J. Miettinen: *CALPHAD*, 2008, vol. 32, pp. 389–98.